Canadian Chemical Transactions

ISSN 2291-6458 (Print), ISSN 2291-6466 (Online)
Year 2014 | Volume 2 | Issue 3 | Page 327-342

Research Article

DOI:10.13179/canchemtrans.2014.02.03.0112

Theoretical Study of the Stability of Tautomers and Conformers of Isatin-3-Thiosemicarbazone (IBT)

Esha Kohli, Ritu Arora and Rita Kakkar*

Computational Chemistry Group, Department of Chemistry, University of Delhi, Delhi-110 007, India

Corresponding Author, E-mail: rkakkar@chemistry.du.ac.in

Received: *April 2, 2014* ***Revised:*** *May 12, 2014* ***Accepted:*** *May 13, 2014* ***Published:*** *May 14, 2014*

Abstract: The isatin based thiosemicarbazones exhibit a number of biological applications. In this paper, we explore various rotamers and tautomers of the title molecule using density functional theory at the B3LYP/6-311++G** level. Investigation reveals that one tautomer dominates the gas phase, of which one of the rotamers constitutes 87% of the gas phase population. The *Z* configuration about the imine linkage is satisfactorily accounted for by the C=O…H hydrogen bonding that results in this planar structure. The orientation of the amine group is also explained by N-H…N hydrogen bonding. The weakening of the C=S bond by hyperconjugative interactions and extended conjugation involving the five membered ring are revealed by an NBO analysis. Comparison of computed geometrical parameters and vibrational frequencies with experimental ones shows good correlation.

Keywords: Isatin-3-thiosemicarbazone; Tautomers; Conformers; Density Functional Theory; Natural Bond Orbital

1. INTRODUCTION

The biological activities of isatin and its derivatives have been known for a long time. Isatin itself exhibits a range of actions, such as CNS-MAO inhibition, and sedative, anticonvulsant and anxiogenic activities [1]. Similarly, isatin derivatives are also known to possess a wide spectrum of pharmacological properties, including antihelmintic, antibacterial, anticonvulsant, antifungal, antineoplastic, antiviral, cysticidal, herbicidal, hypotensive and enzymatic inhibition [1-4]. Among these, isatin-derived thiosemicarbazones have raised considerable interest [1,5-12]. Isatin-3-thiosemicarbazone (IBT) and 1-methylisatin-3-thiosemicarbazone (M-IBT) were the first antiviral drugs used in humans [13], and it was proposed that their mode of action may involve metal ion chelation [14]. M-IBT, 1-ethylisatin and 2-hydroxyethyl thiosemicarbazone were determined to be effective antiviral chemoprophylactic agents in tissue cultures, animal studies, and clinical practice [15]. Different derivatives of M-IBT also possess significant anticancer activity [16]. It was also found that isatin-based thiosemicarbazones protect mice against the intracerebral vaccinia virus, while isatin-based semicarbazones were inactive [17]. All the above-mentioned properties of IBT are mainly a result of its chelating ability. Most of the complexes of

ISSN 2291-6458 (Print), ISSN 2291-6466 (Online)
Year 2014 | Volume 2 | Issue 3 | Page 327-342

IBT are known to involve its thione form, thiol form, or thiol-enol form [11,18-22]. Hence, we may conclude that tautomerism affects its chelating properties, and it is worthwhile to study the tautomers and conformers of IBT in order to have a better insight into the chelating ability of the molecule.

Isatin-3-thiosemicarbazone (Figure 1) consists of an isatin ring and a thiosemicarbazone chain. The six and five membered rings of the isatin moiety are planar [19]. In this molecule, there are several potential hydrogen bond donor and acceptor groups, viz., an -NH_2 group, a keto group, an imine linkage (C=N), a hydrazine hydrogen (NH) and a thione (C=S) group. Therefore, the presence of the -NH group adjacent to the keto group, and the -NH and -NH_2 groups adjacent to the thione group (C=S), leads to a large number of possible tautomers (Fig. 1). Theoretical studies on the relative energies at the B3LYP level with the 6-31G(d,p) and LANL2DZ basis sets are available for the tautomers of 5-methoxyisatin-3-(N-cyclohexyl)thiosemicarbazone, which is one of the derivatives of isatin-3-thiosemicarbazone [23], but, to our knowledge, no such study is available for IBT itself. In the present work, we have performed a DFT study of all the tautomers and conformers of IBT in both the gas and aqueous phases.

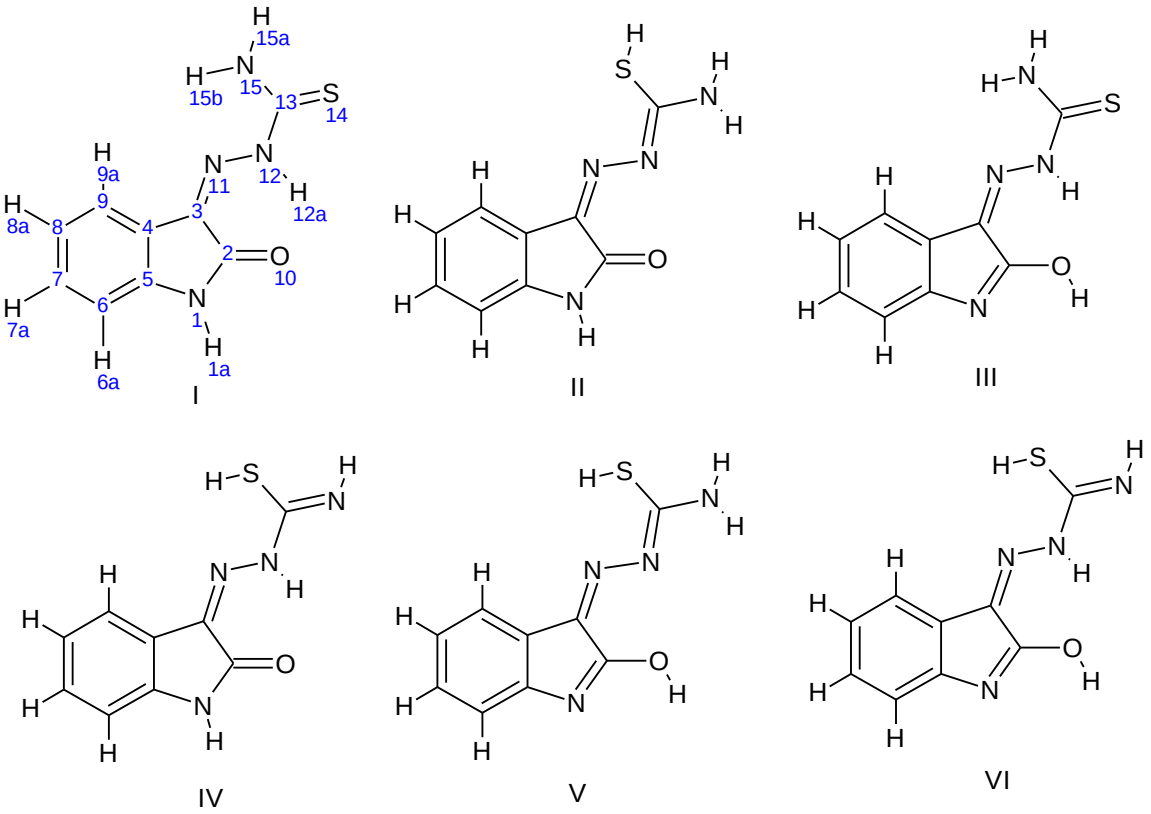

Figure 1. Possible tautomers of isatin-3-semicarbazone (IBT)

2 COMPUTATIONAL METHODS

Because of the presence of several rotatable bonds, several conformers are possible for each of the tautomers of IBT shown in Figure 1. We first performed a conformational search for each tautomer in order to identify the low energy thermally accessible conformations. This was done using the highly efficient Monte Carlo Multiple Minimum (MCMM) approach [24] with the MMFFs force field [25]. The MCMM protocol searches the entire potential energy surface (PES) for low energy minima. The algorithm uses a starting geometry, randomly varies some of the torsion angles and minimizes the

ISSN 2291-6458 (Print), ISSN 2291-6466 (Online)
Year 2014 | Volume 2 | Issue 3 | Page 327-342

resulting structure. This is then compared with previously obtained structures for redundancy by superimposing the heavy atoms. If the Root Mean Square Deviation (RMSD) is less than or equal to 0.5 Å, the structure is rejected as a duplicate and the process continued. Only the low energy structures are used as starting geometries for further steps, and these are used uniformly. The procedure is terminated when no further low energy structure is obtained. Convergence is also judged from the number of times the Global Energy Minimum (GEM) is found in the MC procedure. Only structures within 20 kJ mol^{-1} of the GEM were used as starting geometries in this work. The 20 kJ mol^{-1} energy window was considered sufficient, since only those conformers which are within 5 kJ mol^{-1} of the GEM are likely to be present at room temperature according to the Boltzmann equation. We thus obtained a total of 35 conformationally diverse structures, distributed as follows: 3 for tautomer **I**, 6 for **II**, 2 for **III**, 5 for **IV**, 10 for **V** and 9 for **VI**. These structures were then subjected to more accurate computations using Density Functional Theory (DFT) with the B3LYP hybrid functional [26], implemented in Jaguar 7.6 (Schrödinger, LLC).

It was ascertained that the normal-mode analysis for each final structure revealed no imaginary frequencies. The vibrational frequencies were scaled by a factor of 0.9679 and the zero-point energies by 0.9877 [27] to account for the anharmonicity corrections, and the scaled zero-point energies were added to the calculated energies to give the final energies. Thermochemical analysis at 298.15 K and 1 atm pressure was carried out using these vibrational frequencies assuming ideal gas behavior to account for thermal contributions to the internal energies and enthalpies, as well as entropy contributions to the Gibbs energies. The NBO (Natural Bond Orbital) [28] method was used to identify the best resonance structure of IBT.

Aqueous phase calculations were performed using a self-consistent reaction field (SCRF) method. The solvent was described by the Poisson-Boltzmann SCRF [29], with the dielectric constant (ε) taken as 80.37 for water. PB-SCRF is a continuum solvation model, where the molecule is put into a reaction field consisting of surface charges on a solvent accessible surface constructed using a hypothetical spherical solvent probe molecule with a radius set at 1.40 Å for water. In this method, the wave function and the reaction field charges are solved iteratively until self-consistency is achieved. This method has been found to give accurate solvation energies, with mean errors of 2 – 3 kcal mol^{-1}, even while modeling anions [30]. Furthermore, continuum methods such as this offer many advantages over explicit solvent methods whereas explicit solvent methods suffer from convergence problems, and different starting geometries of the solvent or longer simulation times often produce different final energies. Complete geometry optimizations with no restraints were performed for the aqueous phase. UV-Vis spectra were calculated using the Time-Dependent DFT (TD-DFT) approach [31-33]. All computations were performed using the Schrödinger 2009 suite.

3 RESULTS AND DISCUSSION

3.1 Relative Energies in Gas Phase and Aqueous Solution

All low energy conformers of the various tautomers of isatin-3-thiosemicarbazone (IBT), revealed by the MMFFs calculation, and optimized at the B3LYP/6-31G** level, are displayed in Table A1 (Supplementary Information), which also lists their calculated relative energies with respect to the gas phase conformer **I(a)**, for both the gas phase and the aqueous phase. These calculations were performed with the B3LYP/6-31G** procedure, and no zero-point vibrational energy corrections were applied at this stage.

It is clear that, apart from tautomer **I**, no other tautomer is likely to exist at room temperature, since tautomer **II**, which is closest in energy to **I**, has a relative energy of 17 kcal mol^{-1}, implying that the ratio of the populations of **II** and **I** at room temperature is negligible (~0.001). However, some other

ISSN 2291-6458 (Print), ISSN 2291-6466 (Online)
Year 2014 | Volume 2 | Issue 3 | Page 327-342

tautomers may also show chelating properties [11,18-22]. Because of the large number of tautomers [23] and conformers of IBT, we discuss each one of them in detail and consider their relative stabilities, both in the gas phase and in the aqueous phase. The most stable rotamer of each tautomer is shown in Figure 1, along with the numbering scheme.

Tautomer I

This is the key tautomer and comprises the gas phase population almost exclusively. Various conformers of this tautomer are generated by rotation around the C3-N11 and N12-C13 bonds (Figure 1). The gas phase is dominated by Tautomer **I(a)**, which, according to the Boltzmann distribution law, exists to the extent of ~87%, along with small quantities of **I(b)** (~9%), and **I(c)** constitutes the remaining population (~4%). The overwhelming stability of conformer **I(a)** (Table A1) may be explained on the following basis:

(i) Firstly, the formation of a six membered ring, as a result of intramolecular hydrogen bonding between the ketonic oxygen (O10) and hydrazinic hydrogen (H12a) [34,35]. This factor is also responsible for the existence of the conformer in the Z configuration around the C3-N11 bond [35]. The existence of hydrogen bonding is supported by the calculated value of the distance (2.0 Å) between O10 and H12a, which is smaller than the sum of the van der Waals radii of oxygen and hydrogen (2.68 Å) [36]. The strength of hydrogen bonding (5.7 kcal mol^{-1}) in tautomer **I(a)** is calculated by the difference in the energy of this conformer and the conformer having *E* configuration about the C3-N11 bond (**I(b)**). The hydrogen bond is stronger than the usual value of 2.0 kcal mol^{-1} for N-H...O hydrogen bonds.

(ii) Secondly, the smaller overlap of the lone pair of electrons on N11 and S14, which leads to lesser interelectronic repulsions. Also, the *Z* configuration around the C3-N11 bond minimizes the steric clash between H9a and H12a [35].

(iii) Thirdly, the existence of a five membered ring, formed as a result of intramolecular hydrogen bonding between N16 and H15b [19,34], which is confirmed by their smaller non bonded distance (2.234 Å) as compared to the sum of their van der Waals radii (2.74 Å) [36], stabilizes **I(a)**. The strength of hydrogen bonding between N11 and H15b (7.7 kcal mol^{-1}) is calculated by the difference in energies between **I(a)** and **I(c)**, in which this hydrogen bond is lacking. Again, this hydrogen bond is stronger than the usual N-H...N hydrogen bond of strength 3 kcal mol^{-1}. Aqueous solvation stabilizes the tautomer by 16.5 kcal mol^{-1}.

Tautomer II

Six conformers exist for this tautomer, corresponding to rotation around the C3-N11 and N12-C13 bonds and different orientations of the thiol group (Figure 1). Conformer **II(d)** (Table A1) is the most stable form in both the gas phase and in aqueous solution. It is 17.0 kcal mol^{-1} higher in energy than the global minimum in the gas phase and 18.2 kcal mol^{-1} less stable than the global minimum in the aqueous phase. The stability of **II(d)** compared to the other conformers may be explained on the basis of the following:

(i) Firstly, the existence of intramolecular hydrogen bonding between N11 and H12a, which is confirmed by the larger SH bond length (1.365 Å) in **II(d)** with respect to the SH bond length (1.348 Å) in methyl mercaptan. The larger SH bond length in the gas phase than in the aqueous phase (1.360 Å) suggests the existence of stronger hydrogen bonding in the former. This explains the difference in the relative energy of **II(d)** in the two phases. Also, the distance between H12a and N11 (1.998 Å) is much smaller than the sum of the van der Waals radii of hydrogen and nitrogen (2.74 Å) [36], further confirming the presence of intramolecular hydrogen bonding.

ISSN 2291-6458 (Print), ISSN 2291-6466 (Online)
Year 2014 | Volume 2 | Issue 3 | Page 327-342

(ii) Secondly, minimized interelectronic repulsions of the lone pairs located on the N12, O10 and S14 atoms.

Both these factors contribute to the stability of **II(d)**. Most of the complexes of the thiol tautomer of IBT are known with conformers **II(d)** and **II(e)**, which may be explained by the higher stability of these two conformers in the aqueous phase.

Tautomer III

Unlike the other tautomers, there are only two conformers (Table A1) that are possible for this tautomer. These conformers differ in the arrangement of groups around the C3-N11 and N12-C13 bonds, and conformer **III(a)** (Table A1) is slightly more stable than the other conformer **III(b)**, due to the existence of hydrogen bonding between the hydroxyl oxygen (O10) and the hydrazinic hydrogen (H12a), as evidenced by the small distance (2.084 Å) between the hydroxyl oxygen and the hydrazinic hydrogen.

Tautomer IV

Five conformers (Table A1) are possible for this tautomer, corresponding to different arrangements of groups around the N15-C13 bond, and the different orientations of the SH group. The greater stability of **IV(b)** (Table A1) in the gas phase is associated with reduced interelectronic repulsions of the lone pairs on the N11, S14 and N15 atoms, and the presence of intramolecular hydrogen bonding between H15a and N11.This is supported by the small distance (2.174 Å) between H15a and N11. The steric clash between the H12a, H15a and H15b atoms is minimized in **IV(b)**. However, the order of stabilities of **IV(b)** and **IV(d)** is reversed in the aqueous phase.

Tautomer V

Various conformers for this tautomer arise as a result of rotation around the C3-N11 and N12-C13 bonds and the different orientations of SH and OH groups. Ten conformers (Table A1) are possible for this tautomer. Conformer **V(d)** is stable, both in the gas phase and aqueous phase, due to the intramolecular hydrogen bonding between H1a and N12. The elongation of the OH bond of **V(d)** (bond length = 0.987 Å) with respect to methanol (bond length = 0.961 Å) supports the existence of an intramolecular hydrogen bond between H1a and N12 in the gas phase. This conformer is further stabilized due to the presence of hydrogen bonding between H12a and N11, as reflected in the higher SH bond length in **V(d)** (1.361 Å) with respect to the SH bond length (1.348Å) of methyl mercaptan.

Tautomer VI

For tautomer **VI**, nine conformers (Table A1) differing in the arrangement of groups about the C3-N11 and C13-N15 bonds, along with the different orientations of the SH and OH groups, are feasible. The greater stability of **VI(b)** in the gas phase is associated with hydrogen bonding between H12a and O10. The existence of hydrogen bonding is supported by the small distance between H12a and O10 atoms (2.101 Å). Also the configuration of **VI(b)** minimizes repulsions of the lone pairs of electrons situated on S14, N11 and N15. This configuration also reduces steric clash between H9a and H12a.The existence of intramolecular hydrogen bonding between H15a and N11 further stabilizes **VI(b)**. This hydrogen bonding is confirmed by the reduced non-bonded distance of N11 and H15a (2.180 Å) as compared to the sum of their van der Waals radii (2.74 Å).

3.2 Properties of IBT

Based on the above results, it can be concluded that conformer **I(a)** is the best representation of IBT, as it accounts for 87% of the population in the gas phase. The rest of the gas phase comprises the other two conformers of Tautomer **I**. In addition to **I(a)**, conformers **I(c)**, **II(d)**, **II(e)** and **V(h)** of IBT are responsible for the chelating properties of the molecule [11,18-22]. Hence, we re-optimized the geometry of all of these conformers with a higher basis set at the B3LYP/6-311++G** level and calculated their

ISSN 2291-6458 (Print), ISSN 2291-6466 (Online)
Year 2014 | Volume 2 | Issue 3 | Page 327-342

vibrational frequencies at the same level. The calculated B3LYP/6-311++G** vibrational frequencies were used to confirm the nature of all stationary point structures and to account for the zero-point vibrational energy contribution. The calculated relative Gibbs energy data for these conformers at the B3LYP/6-311++G** level is reported in Table 1.

Table 1. B3LYP/6-311++G** standard Gibbs energies (kcal mol^{-1}) of the conformers and tautomers of IBT in the gas phase and aqueous phase.

Conformer	Relative Gibbs energy	
	Gas phase	Aqueous phase
I(a)	0.0[a]	-16.5
I(c)	3.5	-13.3
II(d)	8.3	-3.9
II(e)	11.5	-1.7
V(h)	22.3	9.7

[a] G^0_{298} = -1040.283877 Ha

Not much difference can be seen between the results of the low-level calculations reported in Table A1 and those reported in Table 1 for the larger basis set, and **I(a)** remains the most stable form of IBT. In the following, we confine ourselves to the study of the properties of this conformer in the gas phase. The largest population of **I(a)** in the solution phase also may be explained by its high dipole moment (6.95 D). Selected bond lengths for **I(a)** are listed in Table 2, along with the experimental values.

Table 2. Selected B3LYP/6-311++G** bond lengths (Å) and bond orders in the gas phase for conformer **I(a).**

Bond	Length		Order
	Calculated	Experimental*	
N12-H12a	1.022	0.83(4)	0.74
C2-O10	1.222	1.235(6)	1.65
C13-S14	1.667	1.663(4)	1.55
C5-N1	1.404	1.398(7)	1.05
N1-C2	1.378	1.350(6)	1.14
N15-H15b	1.009	0.93(6)	0.80
H15b-N11	2.251	2.22(5)	0.01
N11-N15	2.636	2.633(6)	0.01
C3-N11	1.295	1.286(5)	1.62
N11-N12	1.335	1.356(5)	1.20
N12-C13	1.384	1.366(5)	1.10
C13-N15	1.345	1.321(5)	1.25
H12a-O10	2.025	2.09(4)	0.02
N12-O10	2.789	2.730(5)	0.03

*From [34]

Regression analysis between the experimental [34] and theoretical bond lengths yielded an r^2 value of 0.990, which shows that there is only a slight discrepancy between the theoretically calculated bond lengths and the experimental data. This discrepancy is more pronounced in six bond lengths of IBT,

ISSN 2291-6458 (Print), ISSN 2291-6466 (Online)
Year 2014 | Volume 2 | Issue 3 | Page 327-342

viz. N12-H12a, N1-C2, N15-H15b, H15b-N11, H12a-O10 and N12-O10 (Table 2), and may be attributed to the existence of intermolecular hydrogen bonding [34] and crystal packing effects in the solid state, which are otherwise absent in the gas phase. Moreover, the largest variation is for the bonds involving hydrogen and it is well-known that X-ray crystallographic data does not accurately locate their positions. The calculated torsional angles for H9a-C9-C4-C3 (0.1°) and H6a-C6-C5-N1 (0.0°) suggest that the six and five membered rings of the isatin moiety are planar [19,34]. The dihedral angles for C2-C3-N11-N12 (0.2°) and C4-C3-N11-N12 (179.9°) signify the planarity of the thiosemicarbazone chain with respect to the isatin moiety. The dihedral angle for C3-N11-N12-C13 (-179.6°) implies the planarity of the thiourea moiety with respect to the isatin ring.

The computed bond angle corresponding to H12a-N12-C13 (118.5°) suggests that N12 is approximately sp^2 hybridized, which supports the existence of partial double bond character of the N12-C13 bond, as confirmed by the calculated Wiberg bond order (Table 2) of 1.10. Similarly, the bond angles for H15a-N15-C13 (118.3°) and H15b-N15-C13 (120.4°), which are both close to 120°, together with the bond length for the C13-N15 bond, which lies between a C-N bond (1.466 Å) and a C=N bond (1.267 Å), confirms the existence of partial double bond character for the C13-N15 bond, again confirmed by the calculated bond order of 1.25. The bond length for the C13-S14 bond is also intermediate between a C-S bond (1.835 Å) and C=S bond (1.614 Å), and its calculated bond order is 1.55. These observations suggest the involvement of the lone pairs of N15 and N12 in resonance with the adjacent thione group. The bond length for the N11-N12 bond lies between a N-N bond (1.431 Å) and a N=N bond (1.238 Å), which is attributed to the participation of the lone pair of N12 in resonance with the π electron cloud of the adjacent C3-N11 bond, thereby introducing partial double bond character in the N11-N12 bond, as seen from the calculated bond order of 1.20.

The non-bonded distance of 2.025 Å between H12a and O10 atoms is less than the sum of the van der Waals radii of hydrogen and oxygen [36], suggesting the formation of intramolecular hydrogen bonding between O10 and H12a [34,35].This hydrogen bond is responsible for the existence of *Z* configuration around the C3-N11 bond [35]. Also, the non-bonded distance (2.251 Å) corresponding to the N11 and H15b atoms suggests the formation of an intramolecular hydrogen bond between them [34,35] in the same way as in the case of O10 and H12a. This intramolecular hydrogen bond is responsible for the existence of the *E* configuration around the N12-C13 bond [19]. Bond angle data corresponding to the H1a-N1-C2 atoms, and bond length data for the N1-C2 bond (bond order = 1.14), which is intermediate between a C-N bond (1.466 Å) and a C=N bond (1.267 Å), suggests that N1 is approximately sp^2 hybridized and hence confirms the participation of the lone pair of N1 in resonance with the adjacent keto group.

The weakening of the N12-H12a bond (bond order = 0.74) and the interaction of O10 with H12a (bond order = 0.02), confirm the presence of intramolecular hydrogen bonding between O10 and H12a [34,35], as indicated by the bond length data. However, the important point to be noted here is that the weakening of the N12-H12a bond is small, suggested that the intramolecular hydrogen bonding is weak.
Furthermore, the calculated value of the bond order of 1.65 for the C2-O10 bond may be attributed to two reasons. The first is the participation of the lone pair of N1 in resonance with the adjacent keto group, and the second is the formation of intramolecular hydrogen bonding between O10 and H12a [34.35]. Also, the natural population analysis of **I(a)** predicts a natural charge of 0.44 and -0.60 on H12a and O10, respectively, which supports the existence of intramolecular hydrogen bonding between H12a and O10. Reduction in the bond order of the C3-N11 bond is also due to resonance involving the lone pair of the hydrazinic nitrogen (N12) and the π electrons of the C3-N11 bond. The calculated bond orders (Table 3) for the N15-C13, N12-C13 and C13-S14 bonds confirm the participation of the lone pairs of N12 and

ISSN 2291-6458 (Print), ISSN 2291-6466 (Online)
Year 2014 | Volume 2 | Issue 3 | Page 327-342

N15 in resonance with the adjacent thione group. The acidity of the H12a, H15b, H15a and H1a protons is reflected in their respective calculated natural charges (0.44, 0.41, 0.41, 0.41) and in their N-H bond orders (Table 3). Also, the H15b-N11 bond order (0.01) indicates the slight interaction of H15b with N11, which suggests the existence of a very weak intramolecular hydrogen bond between them [34,35].The calculated dipole moment for **I(a)** is 6.95 D and predicts highly polar character of the molecule.
For more detailed understanding of the charge transfer within the system, we carried out an NBO analysis (Table 3).

Table 3. Natural bond orbital (NBO) analysis of **I(a)**.

Donor orbital	Energy	Occ.	Acceptor orbital	Energy	Occ.	Interaction energy (kcal mol^{-1})
n_1(N1)	-0.293	1.661	π* (C6-C5)	0.005	0.377	36.1
n_1(N1)	-0.293	1.661	π* (C2-O10)	-0.018	0.327	59.5
n_2(O10)	-0.290	1.855	σ*(C2-N1)	0.387	0.075	27.0
n_2(O10)	-0.290	1.855	σ*(C2-C3)	0.345	0.086	19.7
n_2 (O10)	-0.290	1.855	σ* (N12-H12a)	0.359	0.042	4.8
n_1(N11)	-0.424	1.925	σ*(C2-C3)	0.345	0.086	12.5
n_1(N11)	-0.424	1.925	σ*(N12-H12a)	0.359	0.042	8.6
n_1(N12)	-0.294	1.592	π*(C3-N11)	-0.024	0.293	39.6
n_1(N12)	-0.294	1.592	π*(C13-S14)	-0.074	0.467	62.1
n_1(N15)	-0.283	1.711	π*(C13-S14)	-0.074	0.467	76.0
n_2(S14)	-0.202	1.878	σ*(N12-C13)	0.373	0.066	12.3
n_2(S14)	-0.202	1.878	σ*(C13-N15)	0.424	0.053	12.3
σ(N15-H15b)	-0.695	1.985	σ*(C13-S14)	0.272	0.012	5.6
π(C9- C4)	-0.273	1.654	π*(C3-N11)	-0.024	0.293	19.3
π(C3- N11)	-0.362	1.863	π*(C2-O10)	-0.018	0.327	12.3
π(C2-O10)	-0.401	1.978	π*(C3-N11)	-0.024	0.293	4.7
π(C3-N11)	-0.362	1.863	π*(C9-C4)	0.013	0.380	9.4
π(C9-C4)	-0.273	1.654	π*(C7-C8)	0.010	0.343	18.2
π(C9-C4)	-0.273	1.654	π*(C6-C5)	0.005	0.377	22.2
π(C6-C5)	-0.285	1.670	π*(C9-C4)	0.013	0.380	16.7
π(C6-C5)	-0.285	1.670	π*(C7-C8)	0.010	0.343	21.0
π(C7-C8)	-0.269	1.668	π*(C9-C4)	0.013	0.380	21.5
π(C7-C8)	-0.269	1.668	π*(C6-C5)	0.005	0.377	17.6

From the NBO analysis, we may conclude that the high occupancy of the π*(C13-S14) orbital is due to the transfer of electron density from the lone pairs of N12 and N15. This results in the weakening of the C=S bond (Table 2). The smaller occupancy of N12 compared with N15 may be explained by the transfer of some of the electron density of N12 to the π*(C3-N11) orbital, which results in the weakening of the C3-N11 bond, which is further weakened by the slight shift of electron density from the π(C9- C4) orbital to the π*(C3-N11) orbital.

The weaker hyperconjugative interaction arising from the donation of electron density from the σ(N15-H15b) orbital to the σ*(C13-S14) orbital also contributes towards the weakening of the C-S bond. The smaller electron density on S14 as compared to N11 is due to larger delocalization of electron density

ISSN 2291-6458 (Print), ISSN 2291-6466 (Online)
Year 2014 | Volume 2 | Issue 3 | Page 327-342

away from S14 to the σ* orbitals of (N12-C13) and (C13-N15).

The lower value of the bond order for the N12-H12a bond may be attributed to the transfer of electron density of the lone pairs situated on N11 and O10 to the σ*(N12-H12a) orbital. The latter interaction and the bond order of 0.02 corresponding to the O10 and H12a atoms supports the formation of intramolecular hydrogen bonding [34,35]. The low occupancy of O10 as compared to N11 is a result of the shift of electron density from the lone pair of O10 to the σ*(C2-N1), σ*(C2-C3) and σ*(N12-H12a) antibonding orbitals. Therefore, C3-N11-N12-H12a-C13-S14-N15-H15b represents the delocalized region.

Electron density from the π(C3-N11) orbital and lone pair of N1 is donated to the π*(C2-O10) orbital, lowering the bond order of the C2-O10 bond to 1.65. Electron density of the lone pair of N1 is also donated to the π*(C6-C5) orbital, further extending the conjugation to embrace the C3-C2-O10-N1-C5 region, along with the aromatic ring. Based on the geometrical parameters, bond orders, charge densities and NBO analysis, we may conclude that the following resonating structures are possible for **I(a)** (Figure 2).

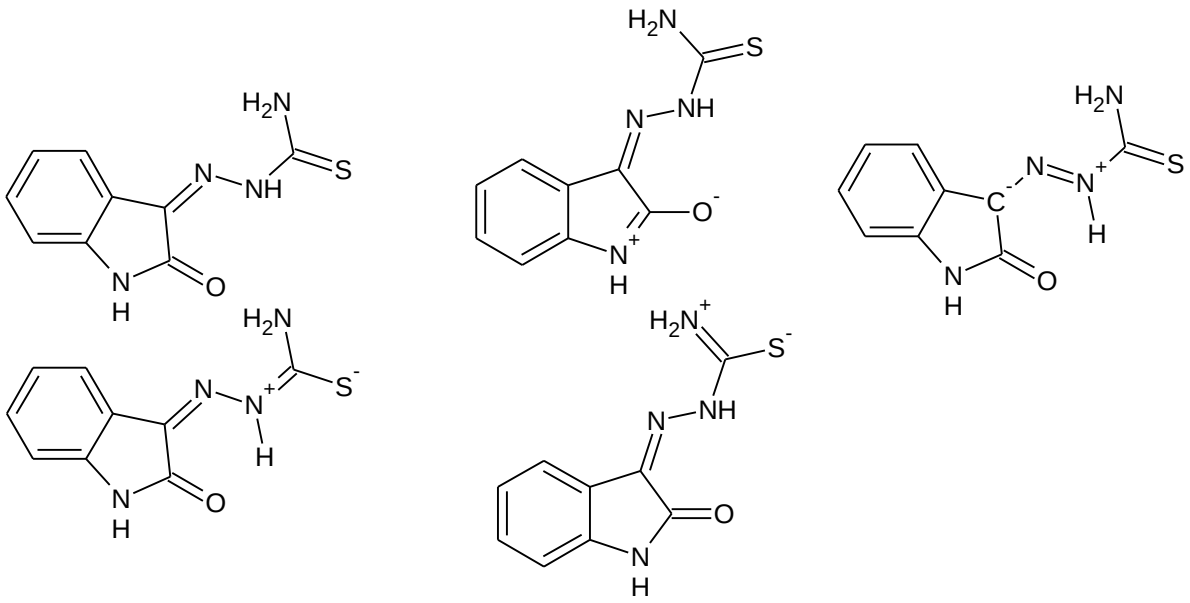

Figure 2. Possible resonating structures of **I(a)** based on the NBO analysis.

The calculated energies of the highest occupied molecular orbital, HOMO (#57) and lowest unoccupied molecular orbital, LUMO (#58) are -0.226 and -0.107 Ha, respectively. The -0.050 Ha isovalue contours for the HOMO (#57) and LUMO (#58) are displayed in Figure 3. It is clear that the HOMO of isatin-3-thiosemicarbazone mainly comprises the nonbonding *p* orbital of S14, and hence this is the electron-rich site of the molecule.

This was further confirmed by the Fukui indices for the molecule, which are reactivity indices, used to identify the atoms in a molecule which have a larger tendency to either lose or gain electrons, i.e. the sites of electrophilic or nucleophilic attack in a molecule. The f_NN index is the partial derivative of the electron density with respect to the number of electrons [37,38]. Usually this is calculated for either the HOMO, in which case it corresponds to the f_- or nucleophilicity index, or the LUMO, for which it corresponds to the f_+ or electrophilicity index. In the present case, this index is maximum in the HOMO for S14 (f_- = 0.91) and, therefore, S14 represents the nucleophilic site in the molecule.

ISSN 2291-6458 (Print), ISSN 2291-6466 (Online)
Year 2014 | Volume 2 | Issue 3 | Page 327-342

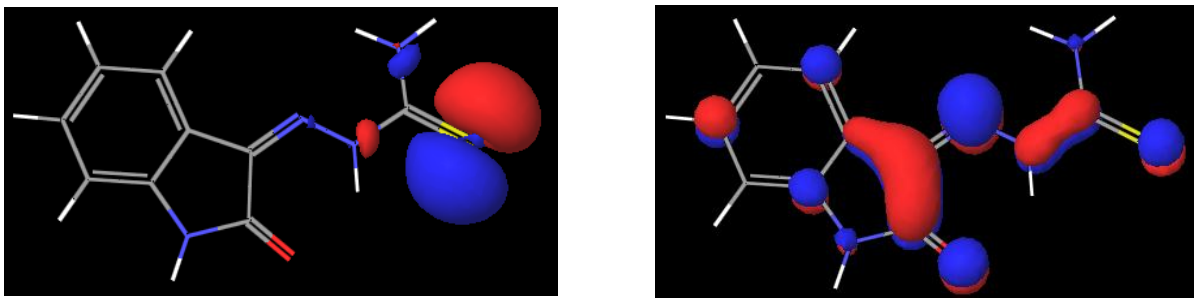

HOMO (#57) LUMO (#58)

Figure 3. Pictorial representation of the HOMO (#57) and LUMO (#58) of IBT.

The LUMO is concentrated in the C4-C3-N11-C2-O10 region and extends to include the N12-C13-S14 region (Fig. 3). The negative LUMO energy signifies that isatin-3-thiosemicarbazone is a good electron acceptor. In contrast to the HOMO, the LUMO represents the electrophilic sites of the molecule. It is clear from Figure 3 that the LUMO mainly involves the π* orbitals of the C3-N11 and C2-O10 bonds, which is further confirmed by the largest values of the atomic Fukui index (f_NN) for the LUMO corresponding to N11 (0.25), C3 (0.13), C2 (0.12) and O10 (0.08) atoms. The LUMO can be classified as a π* orbital because of the presence of a node in the C3-N11 and C2-O10 bonds.

To quantify the reactivity of isatin-3-thiosemicarbazone (IBT), we also determined various global reactivity indices, like the chemical potential, chemical hardness, electrophilicity and nucleophilicity for isatin-3-thiosemicarbazone [39,40]. The vertical ionization potentials (IPs) and electron affinities (EAs) were obtained from the HOMO-LUMO values, which can be used to determine the global electrophilicity value (ω) which is a measure of the energy stabilization when a system acquires an additional electronic charge from the environment [41]. The global electrophilicity value was calculated as $\mu^2/2\eta$, where μ is the chemical potential approximated as -(IP +EA)/2, and η is the chemical hardness approximated as (IP - EA). Chemical hardness measures the resistance to change in the electron distribution in a collection of nuclei and electrons [42]. The calculated values of the chemical potential, chemical hardness and global electrophilicity are -4.53 eV, 3.24 eV and 3.17 eV, respectively. The value of η for isatin-3-thiosemicarbazone is small, which indicates that it is relatively soft on the scale of hardness. The global nucleophilicity model (N) [43,44] is the negative of the gas-phase (intrinsic) ionization potential relative to that of tetracyanoethylene (TCE) (HOMO energy = -0.384 Ha). The calculated value of the nucleophilicity for IBT is 4.30 eV and that for thiosemicarbazide and indole are 4.35 eV and 4.65 eV, respectively, which indicates that IBT is a poorer nucleophile in comparison to indole, but is of comparable nucleophilicity to thiosemicarbazide.

3.3 NMR Spectra

The NMR spectra were calculated at the B3LYP/6-311++G** level in DMSO solvent by using the gauge-independent atomic orbital method [45] that provides magnetic shielding constants. The chemical shifts for selected atoms were obtained on the δ-scale relative to TMS through the equation,

$$\delta_i = \sigma^{TMS} - \sigma_i$$

where the values of σ^{TMS} (31.96 for H and 185.0 for C) were obtained at the same level of calculation (B3LYP/6-311++G**). The experimental [18] and theoretically calculated chemical shifts for ^{13}C and ^{1}H are listed in Table 4.

ISSN 2291-6458 (Print), ISSN 2291-6466 (Online)
Year 2014 | Volume 2 | Issue 3 | Page 327-342

Table 4. Calculated and experimental ^{13}C and ^{1}H chemical shifts (ppm) for IBT.

^{13}C			^{1}H		
Carbon	Experimental*	Calculated	Hydrogen	Experimental*	Calculated
C2	162.6(s)	170.6	H1a	12.45(s)	7.93
C3	132.0(s)	140.0	H6a	6.90(d)	7.36
C4	119.9(s)	127.5	H7a	7.32(t)	7.80
C5	142.3(s)	151.0	H8a	7.05(t)	7.50
C6	111.0(d)	117.7	H9a	7.63(d)	8.11
C7	131.2(d)	139.9	H12a	11.12(s)	12.30
C8	122.3(d)	130.2	H15a	9.01(s)	6.92
C9	120.9(d)	128.4	H15b	8.63(s)	7.80
C13	178.7(s)	189.4			

*From [18]. Figures in parenthesis indicate the multiplicity

A regression analysis of the experimental ^{1}H-NMR and ^{13}C-NMR chemical shifts for **I(a)** with respect to the calculated values yielded the following two equations:

$\delta_{expt.} = 0.591\delta_{calc} + 3.900$ ($r^2 = 0.2411$) (For ^{1}H-NMR)

$\delta_{expt.} = 0.958\delta_{calc} - 2.279$ ($r^2 = 0.9980$) (For ^{13}C-NMR)

The correlation between the theoretical and experimental [18] values for ^{13}C-NMR is excellent, whereas for ^{1}H-NMR, it is very poor. The disagreement is mainly due to H1a and H15a. This may be due to the specific interaction of intermolecular hydrogen bonding of H1a and H15a with the solvent molecules (DMSO), which is not taken into account in the implicit solvent calculations. The ^{1}H-NMR values for H12a and H15b agree well with the experimental values, as they are involved in intramolecular hydrogen bonding [19,34,35] and hence are not very susceptible to interaction with the solvent.

The chemical shift varies with the charge on the atom. Therefore, we performed regression analysis of the experimental chemical shift with respect to the natural charge densities (Table 5) for the C atoms of IBT. The linear fit of the two variables yielded the following equation:

$\delta_{expt.} = 64.6q_C + 134$ ($r^2 = 0.6764$)

The agreement between the calculated chemical shift values using the above linear equation and the experimental ones is not very good, as can be seen from Table 5. We, therefore, fitted the chemical shift with respect to the charge on the corresponding carbon in polynomial equations of higher degrees, and we found a good fit for a polynomial equation of degree four, as given below

$\delta_{expt.} = -4911q_C^4 + 1965q_C^3 + 740.3q_C^2 + 14.62q_C + 119.2$ ($r^2 = 0.9507$)

The resulting chemical shifts (Table 5 and Figure 4) using the above nonlinear equation correlate well with the experimental chemical shifts.

3.4 NICS

To quantify the aromaticity in the ring, we employed the nucleus-independent chemical shift (NICS) method [46], which is a simple and efficient aromaticity probe. NICS is a magnetic index, defined as the negative absolute magnetic shielding computed at the center of the ring. The NICS values were calculated at the center of the ring, i.e. NICS(0) and at a plane 1 Å above it, i.e. NICS(1). In this method, negative NICS values indicate aromaticity and positive values antiaromaticity. The calculated NICS(0) and NICS(1) values for IBT corresponding to the centroid of the fused six membered and five membered ring are negative, -31.5 and -14.5, respectively, which indicate that the molecule is aromatic. The closest aromatic compound with similar structure is indole, for which the corresponding NICS values at 0.0 and

ISSN 2291-6458 (Print), ISSN 2291-6466 (Online)
Year 2014 | Volume 2 | Issue 3 | Page 327-342

1.0 Å above the center of the fused six and five membered rings are -34.9 and -16.6, respectively. Comparison of the NICS(1) values for the two compounds suggests that IBT has 87% aromatic character with respect to indole.

Table 5. Correlation of the experimental chemical shifts (ppm) of carbons for **I(a)** with the computed natural charges.

Carbon	Calculated natural charge	$\delta_{expt.}$	δ_{linear}	$\delta_{nonlinear}$
C2	0.615	162.6	173.7	162.6
C3	0.088	132.0	139.7	127.3
C4	-0.097	119.9	127.7	122.5
C5	0.166	142.3	144.7	147.3
C6	-0.227	111.0	119.3	118.0
C7	-0.181	139.9	122.3	123.9
C8	-0.228	130.2	119.3	117.8
C9	-0.149	128.4	124.4	124.5
C13	0.242	189.4	149.6	177.1

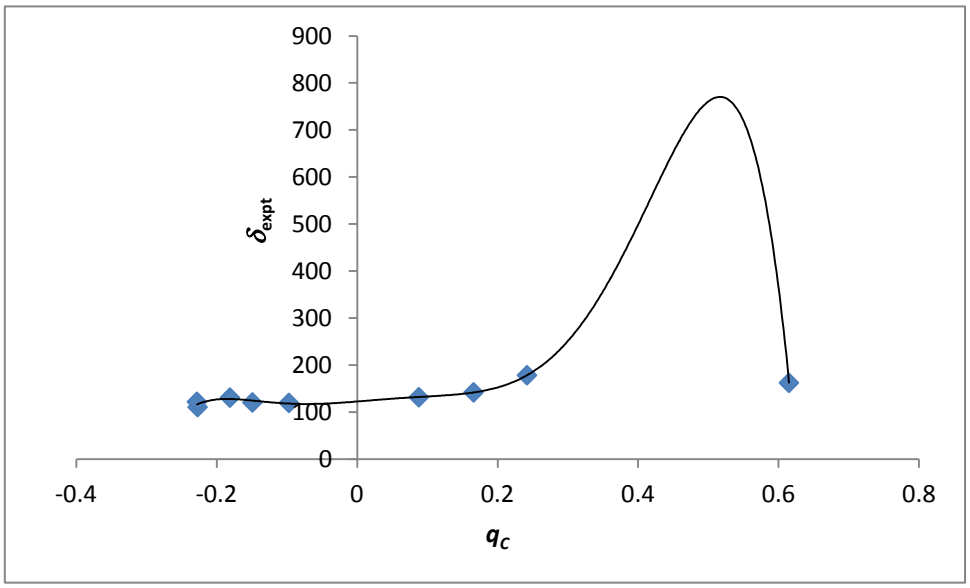

Figure 4. Plot of the experimental ^{13}C chemical shifts (in ppm) versus the computed natural charges on the corresponding carbons, along with the polynomial trendline.

3.5 Electronic Spectra

The calculated UV-Vis spectrum for IBT using the TD-DFT method in vacuum shows λ_{max} values at 309 nm, 395 nm and 263 nm. These values are in good agreement with the experimental UV-Vis spectrum in the solid state (303 nm, 385 nm and 263 nm, respectively) [18].

All the three bands result from the $\pi \rightarrow \pi^*$ transitions of the aromatic ring and the conjugated thiosemicarbazone chain (Table 6). A weak intensity band of wavelength 508 nm corresponding to the $n \rightarrow \pi^*$ transition shows poor agreement with the experimental wavelength (483 nm). This disagreement may be explained by the stabilization of the lone pair located on the heteroatom due to the intermolecular

ISSN 2291-6458 (Print), ISSN 2291-6466 (Online)
Year 2014 | Volume 2 | Issue 3 | Page 327-342

hydrogen bonding in the solid state [34]. The largest contributing orbitals involved in these transitions are reported in Table 6.

Table 6. Calculated and experimental* λ_{max} values (nm) and calculated oscillator strengths for the electronic transitions in IBT.

Orbitals	$\lambda_{expt.}$	$\lambda_{calc.}$	*f*	Transition
54-58	303	309	0.4055	π→π*
56-58	385	395	0.3691	π→π*
56-60	363	263	0.2241	π→π*
57-58	483	508	0.0001	n→π*

*From [18]

3.6 Vibrational Spectra

The experimental [18] and calculated vibrational wavenumbers are reported in Table 7.

Table 7. Calculated and experimental vibrational frequencies (in cm^{-1}) for IBT.

Functional group	Experimental	Calculated*
NH_2(asymm)	3422	3612(115)
N1-H1a	3161	3529(78)
NH_2(symm)	3328	3468(52)
N12-H12a	3264	3326(81)
C=O	1700	1714(296)
C=N	1585	1587(78)
C=S	857	841(70)

*Figures in parenthesis are computed intensities in km mol^{-1}.

The regression analysis of the experimental and calculated vibrational wavenumbers yielded the following equation:

$$\tilde{\nu}_{expt.} = 0.909\tilde{\nu}_{calc.} + 124.2 \quad (r^2 = 0.9920)$$

The maximum deviation between the experimental and theoretically calculated wavenumbers corresponds to the N1-H1a bond and the -NH_2 group (asymm). This may be attributed to the involvement of H1a and H15a in intermolecular hydrogen bonding in the solid state [34].

4. CONCLUSIONS

From the relative energy data, we may conclude that conformer **I(a)** constitutes approximately 87% of the population in the gas phase. A detailed analysis of the geometrical parameters of **I(a)** leads to the conclusion that the six membered benzene ring fused with the five membered ring of the isatin moiety in IBT is planar, and the thiosemicarbazone chain is planar with respect to the isatin moiety. The configuration about the imine linkage (C3-N11) is *Z* due to the existence of intramolecular hydrogen bonding between the H12a and O10 atoms, and *E* about the N12-C13 bond due to the existence of intramolecular hydrogen bonding between H5b and N11.

Resonance occurs between the lone pair of N1 with the adjacent keto group, along with the lone pairs of N12 and N15 with the adjacent thione group. The lone pair of N12 is also involved in resonance with the adjacent π electrons of the C3-N11 bond. The lone pair of the thionic sulphur is the nucleophilic

ISSN 2291-6458 (Print), ISSN 2291-6466 (Online)
Year 2014 | Volume 2 | Issue 3 | Page 327-342

site, and the π* orbital of the iminic linkage (C3-N11), together with the π* orbital of the ketonic group, constitute the electrophilic site of the molecule. IBT is less nucleophilic than indole, and is 87% aromatic with respect to indole.

Correlation of the theoretically calculated ^{1}H-NMR data of IBT with the experimental data suggests the specific interaction of H1a and H15a with the solvent (DMSO). The ^{13}C chemical shift varies as a polynomial of degree four with respect to the charge on the carbon atom. Comparison of theoretical and experimental electronic spectra suggests the involvement of the lone pairs of heteroatoms in intermolecular hydrogen bonding in the solid state. Correlation between experimental and theoretical vibrational frequencies suggests the involvement of H1a and H15a in intermolecular hydrogen bonding in the solid state.

ACKNOWLEDGEMENTS

Financial assistance from "Delhi University's Scheme to Strengthen Research by Providing Funds to Faculty" is gratefully acknowledged. EK and RA gratefully thank the CSIR and UGC, respectively, for providing research fellowships.

REFERENCES

[1] Pandeya, S. N.; Smitha, S.; Jyoti, M.; Sridhar, S. K. Biological activities of isatin and its derivatives. *Acta Pharm*. **2005**, *55*, 27–46.

[2] Beauchard, A.; Ferandin, Y.; Frère, S.; Lozach, O.; Blairvacq, M.; Meijer, L.; Thiéry, V.; Besson, T. Synthesis of novel 5-substituted indirubins as protein kinases inhibitors. *Bioorg. Med. Chem*. **2006**, *14*, 6434–6443.

[3] da Silva, J. F. M.; Garden, S. J.; Pinto, A. C. The chemistry of isatins: a review from 1975 to 1999. *J. Braz. Chem. Soc.* **2001**, *12*, 273-324.

[4] Hyatt, J. L.; Moak, T.; Hatfield, J. M.; Tsurkan, L.; Edwards, C. C.; Wierdl, M.; Danks, M. K.; Wadkins, R. M.; Potter, P. M. Selective inhibition of carboxylesterases by isatins, indole-2,3-diones. *J. Med. Chem.* **2007**, *50*, 1876–1885.

[5] Bal, T. R.; Anand, B.; Yogeeswari, P.; Sriram, D. Synthesis and evaluation of anti-HIV activity of isatin-β-thiosemicarbazone derivatives. *Bioorg. Med. Chem. Lett.* **2005**, *15*, 4451–4455.

[6] Chiyanzu, I.; Hansell, E.; Gut, J.; Rosenthal, P. J.; McKerrow, J. H.; Chibale, K. Synthesis and evaluation of isatins and thiosemicarbazone derivatives against cruzain, falcipain-2 and rhodesain. *Bioorg. Med. Chem. Lett.* **2003**, *13*, 3527–3530.

[7] Chiyanzu, I.; Clarkson, C.; Smith, P. J.; Lehman, J.; Gut, J.; Rosenthal, P. J.; Chibale, K. Design, synthesis and anti-plasmodial evaluation in vitro of new 4-aminoquinoline isatin derivatives. *Bioorg. Med. Chem.* **2005**, *13*, 3249–3261.

[8] Karali, N. Synthesis and primary cytotoxicity evaluation of new 5-nitroindole-2,3-dione derivatives. *Eur. J. Med. Chem.* **2002**, *37*, 909–918.

[9] Karki, S. S.; Thota, S.; Darj, S. Y.; Balzarini, J.; de Clercq, E. Synthesis, anticancer, and cytotoxic activities of some mononuclear Ru(II) compounds. *Bioorg. Med. Chem.* **2007**, *15*, 6632–6641.

[10] Quenelle, D. C.; Keith, K. A.; Kern, E. R. In vitro and in vivo evaluation of isatin-β-thiosemicarbazone and marboran against vaccinia and cowpox virus infections. *Antiviral Res.* **2006**, *71*, 24–30.

[11] Rai, A.; Sengupta, S. K.; Pandey, O. P. Lanthanum(III) and praseodymium(III) complexes with isatin thiosemicarbazones. *Spectrochim. Acta*. **2005**, *61A*, 2761–2765.

[12] Terzioğlu, N.; Karali, N.; Gürsoy, A.; Pannecouque, C.; Leysen, P.; Paeshuyse, J.; Neyts, J.; de Clercq, E. Synthesis and primary antiviral activity evaluation of 3-hydrazono-5-nitro-2-indolinone derivatives. *Arkivoc.* **2006**, *1*, 109–118.

ISSN 2291-6458 (Print), ISSN 2291-6466 (Online)
Year 2014 | Volume 2 | Issue 3 | Page 327-342

[13] Bauer, D. J. Clinical experience with the antiviral drug marboran (1-methylisatin 3-thiosemicarbazone). *Ann. NY. Acad. Sci.* **1965**, *130*, 110–117.
[14] Bauer, D. J. The antiviral and synergic actions of isatin thiosemicarbazone and certain phenoxypyrimidines in vaccinia infection in mice. *Br. J. Exp. Pathol.* **1955**, *36*, 105–114.
[15] [15] Sadler, P. W. Antiviral chemotherapy with isatin β-thiosemicarbazone and its derivatives. *Ann. NY Acad. Sci.* **1965**, *130*, 71–79.
[16] Pandeya, S. N; Dimmock, J. R. Recent evaluations of thiosemicarbazones and semicarbazones and related compounds for antineoplastic and anticonvulsant activities. *Pharmazie.* **1993**, *48*, 659–666.
[17] Thompson, R. L.; Minton, S. A. Jr.; Officer, J. E.; Hitchings, G. H. Effect of heterocyclic and other thiosemicarbazones on vaccinia infection in the mouse. *J. Immunol.* **1953**, *70*, 229–234.
[18] Akinchan, N. T.; Drożdżewski, P. M.; Holzer, W. Syntheses and spectroscopic studies on zinc(II) and mercury(II) complexes of isatin-3-thiosemicarbazone. *J. Mol. Struct.* **2002**, *641*, 17–22.
[19] Bain, G. A.; West, D. X.; Krejci, J.; Valdés-Martínez, J.; Hernández-Ortega, S.; Toscano, R. A. Synthetic and spectroscopic investigations of N(4)-substituted isatin thiosemicarbazones and their copper(II) complexes. *Polyhedron*. **1997**, *16*, 855–862.
[20] Biyala, M. K.; Sharma, K.; Swami, M.; Fahmi, N.; Singh, R. V. Spectral and biocidal studies of palladium(II) and platinum(II) complexes with monobasic bidentate Schiff bases. *Transition Met. Chem*. **2008**, *33*, 377–381.
[21] Konstantinović, S. S.; Radovanović, B. C.; Todorović, Z. B.; Ilić, S. B.; Konstantinović, B. V. Spectroscopic and thermodynamic studies of complexation of some divalent metal ions with isatin-β-thiosemicarbazone. *Chem. Pap*. **2007**, *61*, 485-489.
[22] Rodríguez-Argüelles, M. C.; Sánchez, A.; Ferrari, B. M.; Fava, G. G.; Pelizzi, C.; Pelosi, G.; Albertini, R.; Lunghi, P.; Pinelli, S. Transition-metal complexes of isatin-β-thiosemicarbazone. X-ray crystal structure of two nickel complexes. *J. Inorg. Biochem.* **1999**, 73, 7-15.
[23] Kandemirli, F.; Arslan, T.; Karadayı, N.; Ebenso, E. E.; Köksoy Baybars. Synthesis and theoretical study of 5-methoxyisatin-3-(N-cyclohexyl)thiosemicarbazone and its Ni(II) and Zn(II) complexes. *J. Mol. Struct.* **2009**, *938*, 89–96.
[24] Chang, G.; Guida, W. C.; Still, W. C. An internal-coordinate Monte Carlo method for searching conformational space. *J. Am. Chem. Soc.* **1989**, *111*, 4379-4386.
[25] (a) Halgren, T. A. Merck molecular force field. I. Basis, form, scope, parameterization, and performance of MMFF94. *J. Comput. Chem.* **1996**, *17*, 490-519. (b) Halgren, T. A. Merck molecular force field. II. MMFF94 van der Waals and electrostatic parameters for intermolecular interactions. *J. Comput. Chem.* **1996**, *17*, 520-552. (c) Halgren, T. A. Merck molecular force field. III. Molecular geometries and vibrational frequencies for MMFF94. *J. Comput. Chem.* **1996**, *17*, 553-586. (d) Halgren, T. A. Merck molecular force field. V. Extension of MMFF94 using experimental data, additional computational data, and empirical rules. *J. Comput. Chem.* **1996**, *17*, 616-641. (e) Halgren, T. A.; Nachbar, R. B. Merck molecular force field. IV. Conformational energies and geometries for MMFF94. *J. Comput. Chem.* **1996**, *17*, 587-615.
[26] (a) Becke, A. D. A multicenter numerical integration scheme for polyatomic molecules. *J. Chem. Phys.* **1988**, ***88,*** 2547-2553. (b) Becke, A. D. Density-functional exchange-energy approximation with correct asymptotic behavior. *Phys. Rev. A: At. Mol. Opt. Phys.* **1988**, *38*, 3098-3100. (c) Vosko, S. H.; Wilk, L.; Nusair, M. Accurate spin-dependent electron liquid correlation energies for local spin density calculations: a critical analysis. *Can. J. Phys*. **1980**, *58*, 1200-1211.
[27] Andersson, M. P.; Uvdal, P. New scale factors for harmonic vibrational frequencies using the B3LYP density functional method with the triple-ζ basis set 6-311+G(d,p). *J. Phys. Chem. A* **2005**, *109*, 2937-2941.
[28] Glendening, E. D.; Reed, A. E.; Carpenter, J. E.; Weinhold, F. NBO Version 3.1, **2003**.
[29] (a) Marten, B.; Kim, K.; Cortis, C.; Friesner, R. A.; Murphy, R. B.; Ringnalda, M. N.; Sitkoff, D.; Honig, B. A new model for calculation of solvation free energies: Correction of self-consistent reaction field continuum dielectric theory for short range hydrogen-bonding effects. *J. Phys. Chem.* **1996**, *100*, 11775-

ISSN 2291-6458 (Print), ISSN 2291-6466 (Online)
Year 2014 | Volume 2 | Issue 3 | Page 327-342

11788. (b) Tannor, D. J.; Marten, B.; Murphy, R.; Friesner, R. A.; Sitkoff, D.; Nicholls, A.; Ringnalda, M.; Goddard, W. A.; Honig, B. Accurate first principles calculation of molecular charge distributions and solvation energies from ab initio quantum mechanics and continuum dielectric theory. *J. Am. Chem. Soc.* **1994**, *116*, 11875-11882.

[30] Ahlquist, M.; Kozuch, S.; Shaik, S.; Tanner, D.; Norrby. P. O. On the performance of continuum solvation models for the solvation energy of small anions. *Organometallics* **2006**¸*25*, 45-47.

[31] Bauernschmitt, R.; Ahlrichs, R. Treatment of electronic excitations within the adiabatic approximation of time dependent density functional theory. *Chem. Phys. Lett.* **1996**, *256*, 454-464.

[32] Casida, M. E.; Jamorski, C.; Casida, K. C.; Salahub, D. R. Molecular excitation energies to high-lying bound states from time-dependent density-functional response theory: characterization and correction of the time-dependent local density approximation ionization threshold. *J. Chem. Phys.* **1998**, *108*, 4439-4449.

[33] Stratmann, R. E.; Scuseria, G. E.; Frisch, M. J. An efficient implementation of time-dependent density-functional theory for the calculation of excitation energies of large molecules. *J. Chem. Phys.* **1998**, *109*, 8218-8224.

[34] Casas, J. S.; Castiñeiras, A.; Rodríguez-Argüelles, M. C.; Sánchez, A.; Sordo, J.; Vázquez-López, A.; Vázquez-López, E. M. Reactions of diorganotin(IV) oxides with isatin 3- and 2-thiosemicarbazones and with isatin 2,3-bis(thiosemicarbazone): influence of diphenyldithiophosphinic acid (isatin = 1H-indole-2,3-dione). *J. Chem. Soc., Dalton Trans*. **2000**, 4056–4063.

[35] Stunzi, H. Derivatives of isatin in aqueous solution. II. Z-E isomerism in isatin β-thiosemicarbazones. *Aust. J. Chem.* **1981**, *34*, 373–381.

[36] Rowland, R. S.; Taylor, R. Intermolecular nonbonded contact distances in organic crystal structures: Comparison with distances expected from van der Waals radii. *J. Phys. Chem.* **1996**, *100*, 7384–7391.

[37] Contreras, R. R.; Fuentealba, P.; Galván, M.; Pérez, P. A. Direct evaluation of regional Fukui functions in molecules. *Chem. Phys. Lett.* **1999**, 304, 405-413.

[38] Chamorro, E.; Pérez, P. Condensed-to-atoms electronic Fukui functions within the framework of spin-polarized density-functional theory. *J.Chem. Phys.* **2005**, 123, 114107-114110.

[39] Kakkar, R.; Singh, C. Theoretical study of the kojic acid structure in gas phase and aqueous solution. *Int. J. Quantum. Chem.* **2011**, *111*, 4318-4329.

[40] Kakkar, R.; Bhandari, M.; Gaba, R. Tautomeric transformations and reactivity of alloxan. *Comput. Theor. Chem.* **2012**, *986*, 14-24.

[41] Parr, R. G; Szentpály, L. V.; Liu, S. Electrophilicity index. *J. Am. Chem. Soc.* **1999**, *121*, 1922-1924.

[42] Pearson, R. G. Chemical hardness and density functional theory. *J. Chem. Sci.* **2005**, *117*, 369-377.

[43] Domingo, L. R.; Chamorro, E.; Pérez, P. Understanding the reactivity of captodative ethylenes in polar cycloaddition reactions. A theoretical study. *J. Org. Chem.* **2008**, *73*, 4615-4624.

[44] Jaramillo, P.; Domingo, L. R.; Chamorro, E.; Pérez, P. A further exploration of a nucleophilicity index based on the gas-phase ionization potentials. *J. Mol. Struct.: Theochem.* **2008**, *865*, 68-72.

[45] Wolinski, K.; Hinton, J. F.; Pulay, P. Efficient implementation of the gauge-independent atomic orbital method for NMR chemical shift calculations. *J. Am. Chem. Soc.* **1990**, *112*, 8251-8260.

[46] Schleyer, P. v. R.; Maerker, C.; Dransfeld, A.; Jiao, H.; Hommes, N. J. R. v. E. Nucleus-independent chemical shifts: a simple and efficient aromaticity probe. *J. Am. Chem. Soc.* **1996**, *118*, 6317-6318.

The authors declare no conflict of interest

© 2014 By the Authors; Licensee Borderless Science Publishing, Canada. This is an open access article distributed under the terms and conditions of the Creative Commons Attribution license http://creativecommons.org/licenses/by/3.0/